Available online at www.sciencedirect.com
ScienceDirect
Trans. Nonferrous Met. Soc. China 30(2020) 1249−1266
Transactions of Nonferrous Metals Society of China
www.tnmsc.cn

# Effect of nano-sized $Al_2O_3$ reinforcing particles on uniaxial and high cycle fatigue behaviors of hot-forged AZ31B magnesium alloy

M. DAREINI, A. H. JABBARI, M. SEDIGHI

School of Mechanical Engineering, Iran University of Science and Technology, Narmak, Tehran 1684613114, Iran

Received 13 June 2019; accepted 18 March 2020

**Abstract:** The effect of hot-forging process was investigated on microstructural and mechanical properties of AZ31B alloy and AZ31B/1.5vol.%$Al_2O_3$ nanocomposite under static and cycling loading. The as-cast alloy and composite were firstly subjected to a homogenization heat treatment at 450 °C and then an open-die forging at 450 °C. The results indicated that the presence of reinforcing particles led to grain refinement and improvement of dynamic recrystallization. The forging process was more effective to eliminate the porosity in the cast alloy workpiece. Microhardness of the forged composite was increased by up to 80% and 16%, in comparison with those of the cast and forged alloy samples, respectively. Ultimate tensile strength and maximum tensile strain of the composite were improved by up to 45% and 23%, compared with those of the forged alloy in similar regions. These enhancements were respectively 50% and 37% in the compression test. The composite exhibited a fatigue life improvement in the region with low applied strain; however, a degradation was observed in the high applied strain region. Unlike AZ31B samples, tensile, compressive and high cycle fatigue behaviors of the composite showed less sensitivity to the applied strain, which can be attributed to the amount of porosity in the samples before and after the hot-forging.

**Key words:** magnesium matrix nanocomposite; AZ31B alloy; nano-sized $Al_2O_3$; open-die hot-forging; high cycle fatigue; mechanical properties; microstructural evolution

## 1 Introduction

Magnesium and its alloys as the lightest structural metals have various applications in different industries such as automotive, aerospace, electronics, and sports because of their outstanding properties including high specific strength, high energy damping capacity, and suitable machinability. Nevertheless, the use of magnesium alloys in commercially products is usually limited to die-cast components and they are not utilized as load bearing parts. As a result, wrought magnesium alloys own less amount of the market share [1−3]. In comparison with cast alloys, wrought magnesium alloys exhibit better mechanical behavior in the quasi-static and cyclic loading. Therefore, the improvement of strength, ductility, and other mechanical properties could lead to an ever-growing use of magnesium alloys as load bearing components [1,4].

GOU et al [5] implemented cyclic closed-die forging at three temperatures of 350, 400 and 450 °C on AZ31 alloy ingot fabricated by continuous casting method. The microstructural observations showed a significant reduction in the grain size of the forged samples especially at lower temperatures, compared with the as-cast ones. The texture analysis of the forged materials indicated that the basal planes were oriented perpendicularly to the forging direction. Grain size refinement and the orientation of the basal planes caused improvements in the yield stress, the ultimate tensile strength (UTS), and the ductility. TOSCANO et al [6] investigated the effect of low temperature (275 °C) closed-die forging process on

**Corresponding author:** M. SEDIGHI; Tel: +98-2173228975; E-mail: sedighi@iust.ac.ir
DOI: 10.1016/S1003-6326(20)65293-1

the mechanical behavior of AZ31B alloy. Their results exhibited an increase in the yield and ultimate tensile strengths along with a significant improvement in the fatigue life of the forged samples due to the microstructural and texture modifications compared with the as-cast specimens.

Adding reinforcing particles to the magnesium phase can modify mechanical and microstructural properties of the monolithic alloys and increase their applications. Hence, many researchers have recently attempted to produce magnesium matrix composites with improved properties [7−9]. Among all the available methods for production of metal matrix composites, the liquid phase stir-casting procedure is a popular method due to its simplicity and possibility to be used for mass production. In addition, the production cost of this method is about one third in comparison with other competitive methods, which drops up to one tenth in mass production [10,11]. Considering the microstructural defects of cast composites, usually a secondary process such as forging, rolling, and extrusion is employed to remove porosity, modify the microstructure, and consequently improve the mechanical properties of the cast parts [11,12]. It is worth noting that magnesium and its alloys suffer from a limited formability at room temperature due to their hexagonal close packed (HCP) structure. The critical resolved shear stress (CRSS) for basal slip planes system is significantly less than that of non-basal ones (prismatic and pyramidal) at the ambient temperature. Therefore, plastic deformation at temperatures below 200 °C is usually restricted to the basal slip and twinning mechanisms.

Accordingly, in many previous studies, the forming process of magnesium and its composites was carried out at elevated temperatures [2,13]. WANG et al [14] produced AZ31/1vol.%SiC nanocomposite by ultrasonic-assisted stir casting method. Specimens were rolled up to 8 passes after a heat treatment at 400 °C. The rolled composites showed an increase in the yield strength and a ductility reduction due to the nanoparticle bands, lamellar microstructure, and inhibiting the shear bands formation. DENG et al [15] studied the closed-die forging of AZ91 reinforced with 10 vol.% SiC particles (average size of 10 μm). The composites were manufactured by two-step semi-solid stir casting method. After T4 heat treatment, the composites and alloys were forged at 420 °C with 40%−80% height reduction. The results showed that the presence of the ceramic reinforcing phase caused a more grain refinement in the forged composites compared with the alloy samples. Furthermore, by increasing the amount of height reduction, dynamic recrystallization phenomenon was expanded in the matrix. The composites exhibited superior yield stress and UTS and inferior ductility. However, with excessive deformation from 60% to 80%, the increase in the strength has declined slightly due to the formation of particle agglomeration.

GOH et al [16] studied the fatigue behavior of the extruded pure magnesium reinforced with multi-walled carbon nanotubes. The results illustrated that the nanocomposites experienced a lower fatigue lifetime in comparison with the monolithic sample in the same range of the applied plastic strain. The fatigue life reduction was due to the presence of cavities and particle agglomeration. YUAN et al [8] used a combination of ball milling and stir casting processes. This method allowed the carbon nanotubes (CNTs) to be distributed more uniformly inside the melted AZ91D matrix. The proper CNTs distribution, grain size refinement, and strong interfacial bonding resulted in superior yield and ultimate tensile strengths, enhanced elongation, and improved work of fracture in the composite specimen. LIANG et al [17] distributed CNTs in AZ91D matrix using friction stir processing (FSP). Subsequently, the materials were subjected to an ultrasonic assisted melting followed by a high-temperature extrusion. The strength of the composite specimens was improved compared with the alloy ones, whereas the ductility was not considerably reduced. This strength enhancement was due to the high load transfer capability of the CNTs resulted from strong interfacial bonding between the reinforcing and matrix phases. The mechanical properties of the composite decreased due to the particle cluster when the volume fraction of the CNTs was above a threshold of 1%. HASSAN and LEWANDOWSKI [18] developed a composite of AZ91D/SiC (with an average diameter of 15 μm) in various volume fractions using squeeze casting and hot extrusion process. By adding more amount of SiC powders, the yield stress and UTS significantly increased, while the ductility was reduced considerably. Also, fatigue life of the composites in the low cycle region

decreased with increasing SiC volume fraction, but a potential improvement in the high cycle regime was observed. SRIVATSAN et al [19] produced AZ31/1.5vol.%$Al_2O_3$ nanocomposite by DMD (disintegrated melt deposition) method and hot-extrusion process. The composites showed yield stress and UTS augmentation along with a ductility reduction due to the increase of the brittle and hard $Mg_{17}Al_{12}$ secondary phase. Moreover, the presence of the reinforcing particles improved the endurance limit of the composite under fatigue loading.

Considering the possible application of forged magnesium matrix composites, it is essential to study their mechanical behavior under static and cyclic loading. In this regard, a composite of AZ31B magnesium alloy reinforced with $Al_2O_3$ nanoparticles was produced by stir casting and open-die hot-forging processes. Then, the effects of nano-sized particles and also applied strain field during the hot-forging process were investigated on microstructure, microhardness, tensile, compressive, and high cycle fatigue behaviors of the composite. To achieve better understanding, the results were compared to that of monolithic alloy specimens.

## 2 Experimental

Table 1 shows the chemical composition of the AZ31B magnesium alloy employed as the matrix. Nano-sized $Al_2O_3$ ceramic particles with an average diameter of 50 nm and a purity of 99% were used to reinforce the matrix.

**Table 1** Chemical composition of as-received AZ31B magnesium alloy (wt.%)

| Ni | Zn | Al | Mn |
|---|---|---|---|
| 0.0009 | 0.7920 | 3.0300 | 0.3670 |
| Cu | Fe | Si | Mg |
| 0.0011 | 0.0017 | 0.0080 | Bal. |

The composite was fabricated by a novel stir casting technique using both mechanical and electromagnetic stirring methods in the presence of argon gas [20,21]. To modify the dendritic and eutectic structure resulted from the casting process and consequently decrease the precipitation and increase the formability, the as-cast ingots were heated up to 450 °C for 3 h as homogenization heat treatment process. Then, they were cooled to the ambient temperature in the free air.

### 2.1 Open-die hot-forging process

Cylindrical shape specimens with height and diameter of 50 mm were extracted from homogenized ingots using lath machine. Afterwards, the specimens were subjected to a forging process at 450 °C. For this purpose, two flat dies made of AISI H13 (DIN 1.2344) surrounded by electrical resistance heating elements were used. To reduce the friction during forging process, the specimen and dies were impregnated with $MoS_2$-based lubricant. The height reduction in the workpiece was approximately 75%. A hydraulic press was used to implement the process with a ram speed of 5 mm/s. The workpiece photos before and after the hot-forging process are shown in Fig. 1.

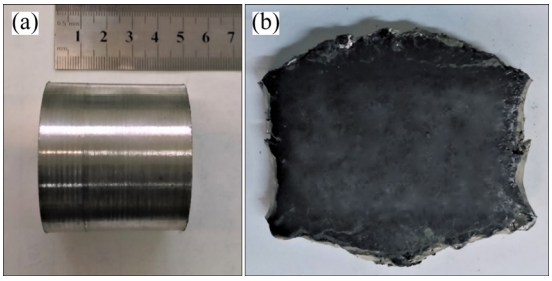


**Fig. 1** Photos of workpiece before (a) and after (b) hot-forging process

### 2.2 Microstructural and mechanical tests

Forged alloy and composite workpieces were cut to prepare required samples for the microstructural and mechanical tests. In order to carry out microstructural evaluation with optical microscope (OM), the samples were cut from the as-cast ingots and the middle of the forged workpieces. Then, the samples were ground with sandpapers up to 2500 grit. The ground samples were mechanically polished using suspensions of aluminum oxide abrasive particles (with average particle sizes of 3, 1, and 0.3 μm). Finally, the samples were etched with an acetic−picral etchant (solution with 4.2 g picric acid, 10 mL acetic acid, 10 mL distilled water, and 70 mL ethanol [7]) for 5 s. Energy dispersive X-ray spectroscopy (EDS) was also used to investigate the chemical composition and the elemental analysis of the materials.

Since the applied plastic strain field is not uniform in the forged workpieces, the

microhardness of the forged alloy and composite samples was investigated at different points of the cross-sections. As shown in Fig. 2, for half of the forged workpiece in a finite element simulation (DEFORM-3D software), the von Mises strain value is the maximum at the midpoint, which decreases in both longitudinal and transverse paths starting from the midpoint. The Vickers micro-hardness was measured at 5 points (with equal intervals of 10 mm) in the longitudinal direction and at 3 points (with equal intervals of 12.5 mm) in the transverse direction. The force of the indenter during the microhardness test was 2 N for a duration of 10 s. For each position, the average values of the measured microhardness (in three trials) were reported.

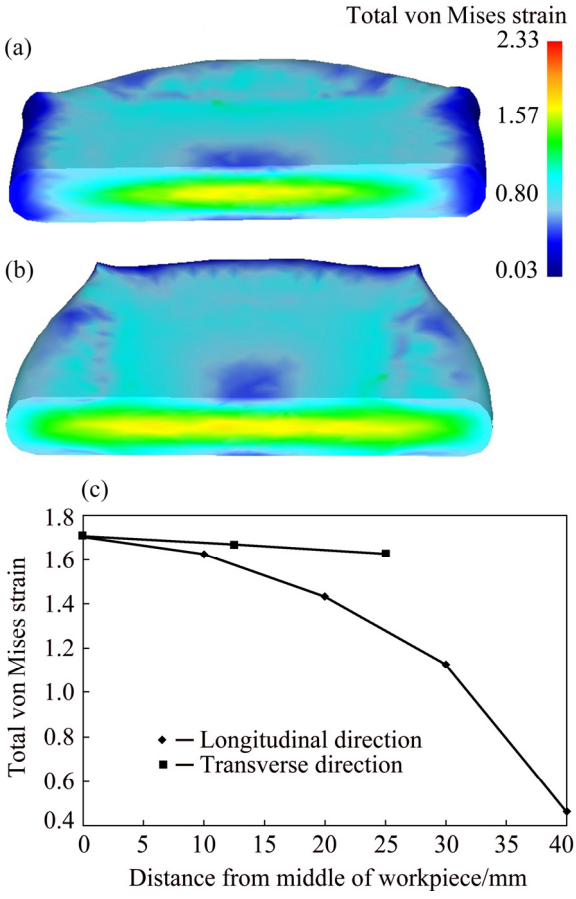


**Fig. 2** Strain contour in half of forged workpiece: (a) Longitudinal direction; (b) Transverse direction; (c) Total von Mises strain at different points

Considering the symmetrical geometry of the forged workpieces and to investigate the effect of applied strain on the mechanical behavior, the samples of uniaxial tensile/compressive and high cycle fatigue tests were extracted from the workpieces according to Fig. 3. As it was demonstrated in Fig. 2, samples near and far from the center of the workpiece experienced a high applied strain (HAS) and a low applied strain (LAS), respectively. After cutting the forged workpiece, the dog-bone samples of the tensile/fatigue tests and the cylindrical samples of the compressive test were machined to achieve the desired geometries [3]. The uniaxial tensile and compressive tests were performed using Santam-STM50 apparatus at room temperature and a strain rate of 0.001 $s^{-1}$.

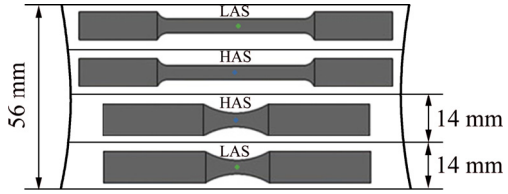


**Fig. 3** Schematic positions of uniaxial tensile and HCF test samples extracted from forged workpiece

A Santam SFT−600 rotating-bending fatigue machine with a constant rotational speed of 6000 r/min was used to carry out stress-controlled high cyclic fatigue tests under completely reversible loading ($R$=−1, $R$ is the stress ratio) and at the ambient temperature. The stress amplitudes ($\sigma_a$) were selected between 30 and 100 MPa and the number of cycles to failure ($N_f$) was reported as the fatigue life. If the sample passed $1\times10^7$ cycle without failure, the test was stopped and it was considered as an infinite fatigue life. At the end, a scanning electron microscope (VEGA−II TESCAN) was used to observe the fracture surfaces of the tensile and fatigue test samples.

## 3 Results and discussion

### 3.1 Microstructure

Figure 4 illustrates the OM and SEM images of the cast alloy and composite samples after stir casting and heat treatment processes.

According to the OM images, the alloy sample has a coarser grain size (even in millimeter order) which is due to the nature of the casting and the heat treatment processes. As it can be observed, the grain size is decreased considerably in the composite sample in comparison with the cast alloy. There is also no evidence of large particle agglomeration in the matrix in the large-scale

images, although the presence of the particle agglomeration and clusters in lower scales is not preventable due to the nature of the casting process, solidification conditions, and poor wettability especially around nano-sized particles with high specific surface area [22].

The grain size refinement in the composite can be attributed to the several factors. Firstly, the presence of the nano-sized ceramic particles increases the grain nucleation sites during the solidification [19,23−25]. Further, in accordance with Zener pinning effect, hard particles as strong barriers can reduce grain size by inhibiting grain growth during solidification or hot work [26,27]. Figures 4(c) and (d) illustrate the intermetallic secondary phases and the porosity in the SEM images of the cast alloy and composite microstructures, respectively. It is clear that large shrinkage cavities were locally formed (especially on the edges) in the AZ31B alloy sample, while the presence of $Al_2O_3$ reinforcing particles in the composite led to changing them to a uniform micro-porosity in all regions of the ingot. Table 2 shows the densities and porosities of all the cast and forged alloy and composite samples measured by Archimedes principle.

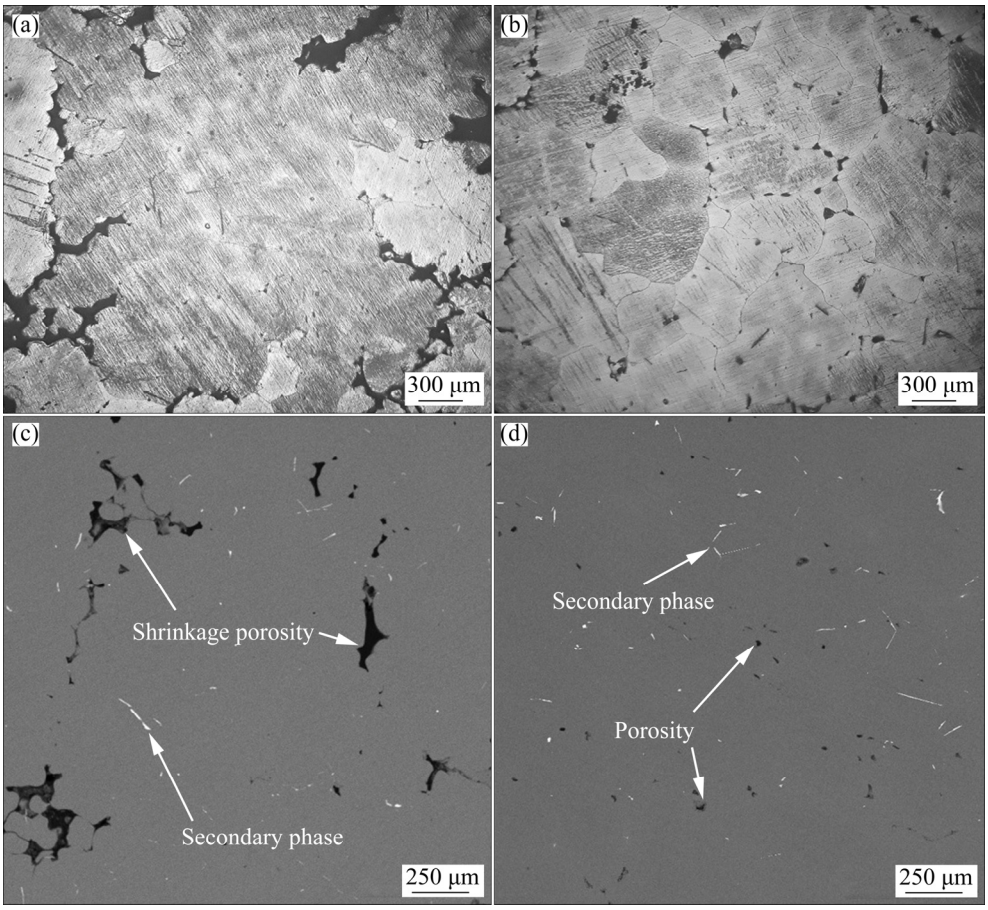


**Fig. 4** OM (a, b) and SEM (c, d) images showing microstructure of homogenized ingots: (a) Etched specimen of alloy; (b) Etched specimen of composite; (c) Porosity and secondary phase in alloy; (d) Porosity and secondary phase in composite

**Table 2** Densities and porosities of alloy and composite samples

| Material | Condition | Theoretical density/ ($kg \cdot m^{-3}$) | Experimental density/ ($kg \cdot m^{-3}$) | Porosity/ % | Porosity reduction/% |
|---|---|---|---|---|---|
| AZ31B alloy | As-cast | 1776 | 1731 | 2.53 | 71 |
| | Forged | 1776 | 1763 | 0.73 | 71 |
| AZ31B/1.5vol.%$Al_2O_3$ composite | As-cast | 1809 | 1746 | 3.46 | 19 |
| | Forged | 1809 | 1758 | 2.80 | 19 |

According to Table 2, the porosities are 2.53% and 3.46% in the cast alloy and composite, respectively. There are several factors causing porosity formation in the cast materials such as the dissolved gas bubbles entrapment during stirring, the shrinkage in solidification, and the isolated gas inside clusters and agglomerations of reinforcing particles [10,28]. Thus, as expected, the composite specimens contain more porosity compared with the cast alloy [29]. In addition, the open-die forging process reduced the amount of porosity, although this reduction is very more significant in the alloy workpiece. In fact, the porosities of the forged alloy and composite samples decrease to 0.73% and 2.8%, which respectively show 71% and 19% reduction. It is worth noting that applying more plastic strain using other hot forming processes such as closed-die forging or extrusion can decrease the porosity more effectively, especially in the composite ingots [21]. Figure 5 shows the microstructures of

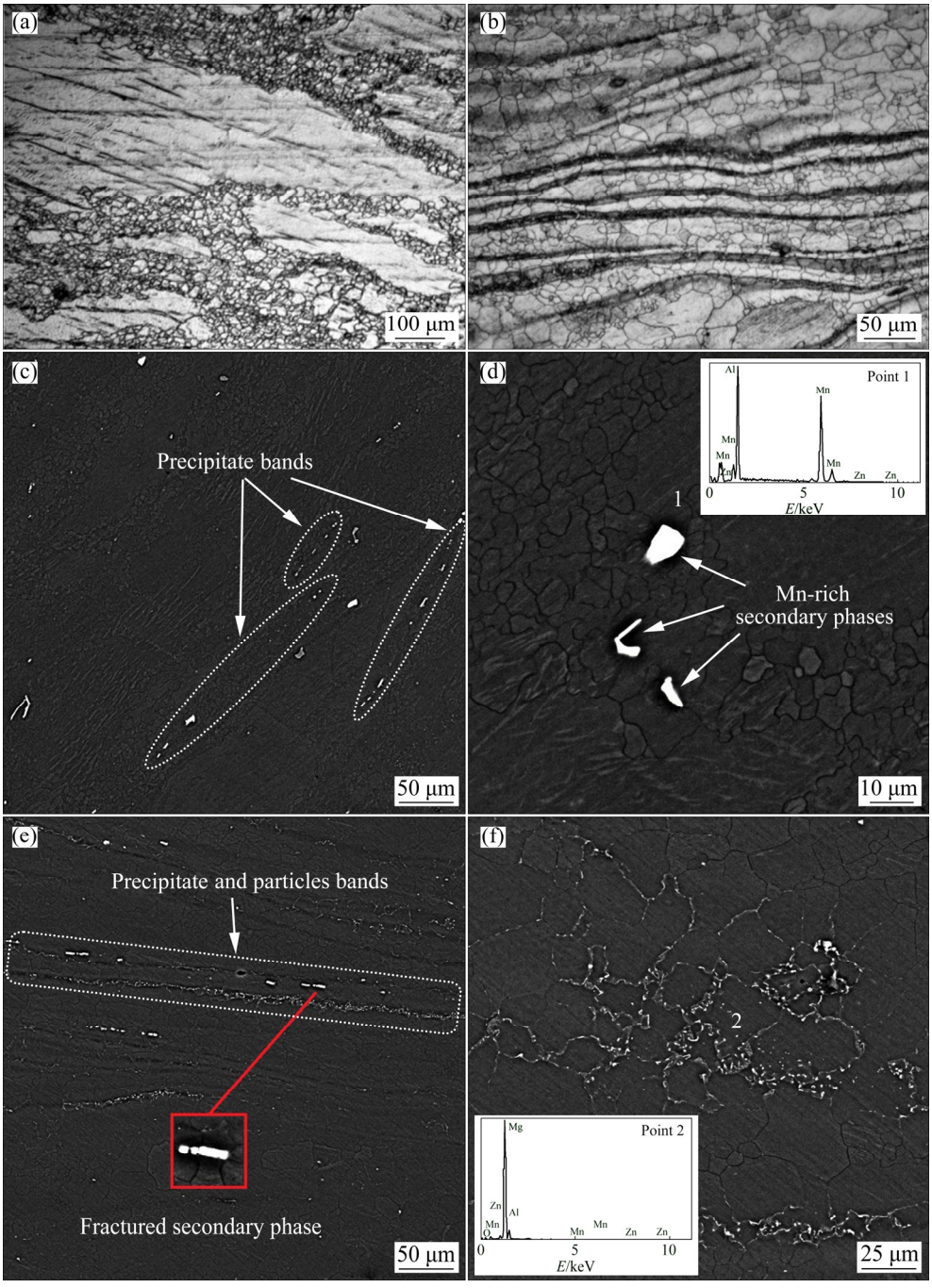


**Fig. 5** Microstructures of forged workpieces: (a) Grain morphology of alloy; (b) Grain morphology of composite; (c) Precipitate bands in alloy; (d) Mn-rich secondary phase in composite; (e) Lamellar microstructure of composite; (f) Particles and precipitate agglomeration in composite

the forged alloy and composite samples. There are bimodal grain size distributions in the two kinds of materials due to the partial dynamic recrystallization (DRX).

According to Figs. 5(a) and (b), finer grains can be observed along the shear bands and the grain boundaries of the forged samples. In brittle materials with HCP crystal lattice such as magnesium alloys, most of the applied strain gradient occurs in the slip planes where the shear stress is the maximum. This strain can modify microstructure and cause grain size refinement due to DRX. During high temperature metal forming processes, dislocation density should reach an extremely critical level in matrix in order to start DRX in microstructure [15,30]. Moreover, when the forming process is done at a relatively high strain rate, the sample formability will be reduced and an incomplete DRX (partial DRX) will happen inside the microstructure of the specimens. Figure 5(a) shows that in the forged alloy sample, DRXed grains were created with an incomplete necklace pattern [2,31,32]. On the other hand, DRX can occur more easily in the composite sample. It has been confirmed that the presence of ceramic reinforcing particles can accelerate dynamic recrystallization phenomenon due to a higher dislocation density and more uniform distribution of the grains [30]. Mismatches of thermal expansion coefficient and modulus of elasticity between the reinforcing particles and the matrix lead to the increase in the dislocation density in the composite. According to Fig. 5(c), open-die forging leads to the formation of secondary phase bands in the plastic flow regions with DRXed grains. The results of EDS elemental analysis of the alloy sample (Fig. 5(d)) demonstrate that the secondary phases contain significant amounts of Mn (between 72 at.% and 82 at.%), indicating the presence of $\beta$-Mn chemical compositions in the magnesium matrix [33,34]. In addition, $Mg_{17}Al_{12}$ intermetallic phase can be observed in the matrix, although its volume fraction decreases meaningfully due to the homogenization heat treatment.

SEM images of the forged composite are presented in Figs. 5(e) and (f). Secondary phase and nano-sized particle bands surrounded by fine DRXed grains are shown in Fig. 5(e). Creation of these bands leads to formation of a lamellar microstructure. Similar lamellar microstructure was observed in the AZ31/SiC composite after accumulative roll bonding [14]. It should be noted that applying high plastic strain during forging process can break particle agglomerations and brittle secondary phases in the bands. Point 2 in Fig. 5(f) consists of particle and precipitate agglomerations. Particle agglomeration usually occurs at grain boundaries. These sites act as barriers to the grain growth during solidification. Furthermore, they create favorable conditions for formation of DRX nucleation sites. As a result, more DRXed grains can be observed around them in the forged samples.

### 3.2 Microhardness

Figure 6 shows the microhardness of the as-cast forged alloy and composite samples in different regions in the longitudinal and transverse directions. The midpoints of both alloy and composite samples own the maximum microhardness compared with other regions. Although the composite specimen offers a higher microhardness at all the points, a similar decreasing trend is observed in the longitudinal and transvers directions for both samples. The microhardness improvement in the nanocomposites reinforced with

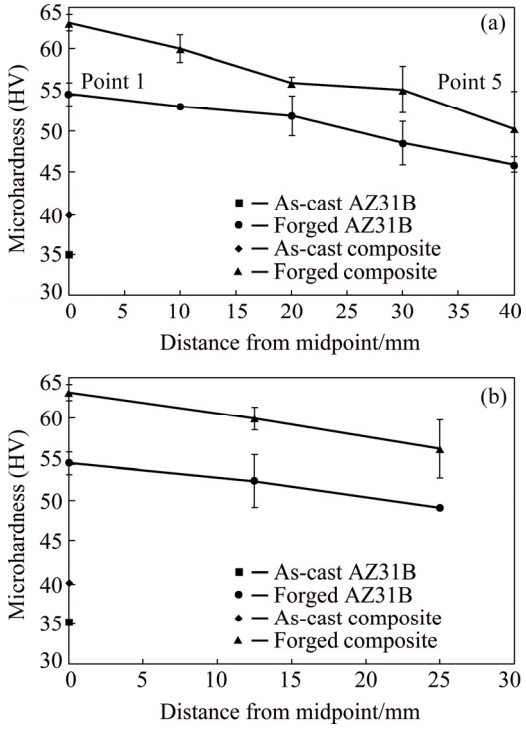


**Fig. 6** Microhardness of as-cast and forged samples at different points: (a) Longitudinal section; (b) Transverse section

ceramic particles occurs due to the finer grains (according to the Hall−Petch strengthening mechanism [24,35]), higher dislocation density, and the role of the particles to act as barriers for dislocation movement and local plastic deformation [19,36].

The results also show that the plastic strain has an important impact on the microhardness of the samples. The microhardness value gradually diminishes by decreasing the applied plastic strain. In longitudinal direction, the microhardness value in the forged composite decreases from HV 63.1 at Point 1 (with equivalent von Mises strain of 1.7) to HV 50.3 at Point 5 (with von Mises strain of 0.5). The corresponding values are HV 54.4 and HV 45.9 for Point 1 and Point 5 in the forged alloy sample, respectively. Less plastic strain leads to less dislocation density and consequently decreases the possibility of DRX occurrence. In addition, more defects such as voids, porosity, and micro-cracks remain in the samples, resulting in a reduction in the microhardness. Considering the microhardness of the samples before the forging process (HV 35 for the alloy and HV 39.7 for the composite), an enhancement of 55% and 59% can be observed in the middle of the alloy and the composite samples, respectively. As expected, the composite exhibits a higher microhardness improvement, which is due to more DRX.

### 3.3 Uniaxial tensile behavior

Figure 7 illustrates the engineering stress−strain curves of the forged alloy and composite samples in two different strain regions (LAS and HAS zones). Since there is not a uniform strain field in the forged workpieces, the open-die hot-forging process leads to a non-homogeneous tensile behavior in the both AZ31B and AZ31B/1.5vol.%$Al_2O_3$ samples. However, the composite sample shows less sensitivity to the applied strain compared with the alloy one. For instance, the UTS of AZ31B-HAS sample is improved by 37% in comparison with that of AZ31B-LAS, while this amount is limited to 6% in the composite samples. Furthermore, the ductility values (in terms of maximum elongation at the breaking point of HAS and LAS samples) are increased by 44% and 34% for the alloy and composite specimens, respectively. Unlike UTS and ductility, the variation of the yield stress is not

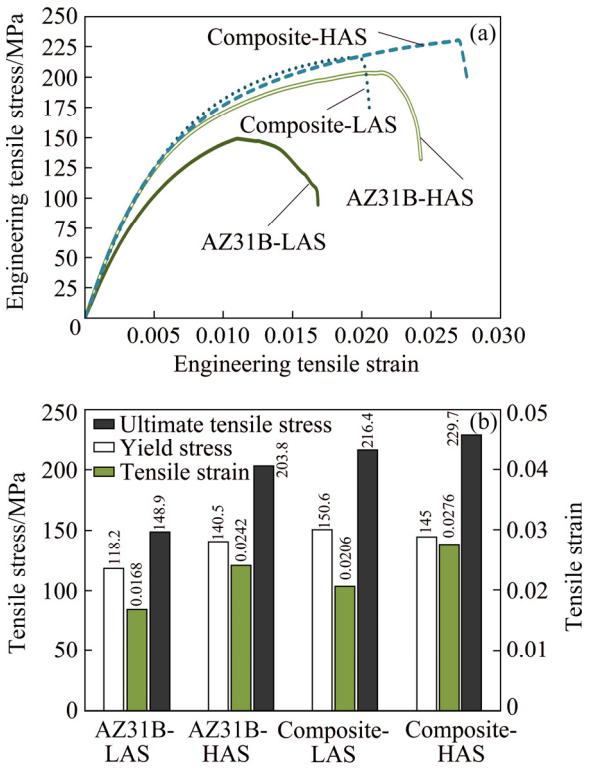


**Fig. 7** Tensile behavior of forged alloy and composite specimens: (a) Engineering tensile stress−strain curves in two different strain regions (LAS and HAS); (b) Yield stress, UTS and tensile strain

considerable in all the samples. The most possible reason can be the implementation of the forging process at an elevated temperature (450 °C), resulting in less work hardening in different applied strains. On the other hand, reduction of the porosity, micro-cracks, and grain size of the as-cast samples during the forging process can be considered as the most important reasons for improvements of the UTS and ductility. According to Table 2, porosity of the alloy sample is reduced by 71% during the hot-forging, while this reduction is approximately 19% in the case of the composite. This confirms that the applied plastic strain is more effective to close the existing voids and porosity in the alloy samples (big and local voids with less volume fraction), in comparison with that of the composite. Due to high porosity in the cast composite (3.46%), in general, the plastic strain during the forging process is not able to reduce its porosity significantly. On the other hand, the forged alloy workpiece experiences a considerable elimination of the porosity. So, the amount of the remained porosity in the alloy workpiece has more

dependency on the applied strain. Since the mechanical properties depend on microstructural defects such as porosity, more sensitivity to the applied strain is observed in the alloy sample.

In addition, the relative improvement in the composite strength can be attributed to the participation of various strengthening mechanisms such as mismatches between the coefficients of thermal expansion (CTE) and elastic moduli of the ceramic particles and the matrix, the Hall−Patch and the Orowan mechanisms, the role of the particles to barrier dislocation movement, and also the increased load bearing capacity due to the existence of the reinforcing particles [12,15,25]. During the cooling process after the hot-forging, difference of the CTE between the magnesium matrix and the ceramic reinforcing phases leads to thermal residual stress at the interfaces, which can result in creation of geometrically necessary dislocations (GNDs) [23,37]. Furthermore, during the deformation, the mismatch of the elastic modulus (strain misfit) between two phases generates dislocations in the matrix. As a result, the strength of the composite increases by enhancing the dislocation density [27,38]. Nano-sized particle in the composite can prevent the dislocations movement, cause dislocation bowing and consequently forming dislocation loops around the non-shearable nanoparticles according to the Orowan looping mechanism. This strengthening mechanism is very common in discontinuous reinforced metal matrix composites containing nanoparticles with a low aspect ratio (close to the unit) [39]. In addition, more grain boundaries in the composite with finer grains have a strengthening effect and can act as a relatively rigid barriers to the dislocation movement and deflect their slipping (Hall−Patch strengthening mechanism) [40].

In general, it is expected that adding hard ceramic reinforcing particles will lead to a reduction in the final elongation [24,41]. Nevertheless, the composite samples show a higher ductility in comparison with the alloy. The most possible reason is the activation of none-basal slip mechanism (especially prismatic planes), which happens due to the presence of the nano-sized particles and consequently postpones the metal premature rupture [13,16,24]. It has been observed that during open-die forging process of magnesium alloys in the radial direction, the *C*-axis of the HCP crystals is oriented approximately parallel to the forging direction [2,42]. But the presence of the reinforcing particles causes a deviation in the *C*-axis direction and weakens the basal texture. So, in addition to the more activation of the deviated basal slip planes which are not preferably oriented in the alloy sample to provide the required strain during the tensile test, non-basal slip mechanism (prismatic) may be also activated during the tension of the specimens (in the direction perpendicular to the forging direction). Moreover, grain size refinement can lead to an increase in ductility of magnesium and its alloys [43].

### 3.4 Uniaxial compressive behavior

Figure 8 shows the engineering compressive stress−strain curves of the forged alloy and composite in different strain regions. Similar to the tensile test, composite specimens offer better behavior than the alloy ones in the compression test. Adding $Al_2O_3$ particles has improved the ultimate compressive strength (UCS) by 49.7% and 25.9% in LAS and HAS samples, respectively. Similar to the tensile behavior, the composite specimens show the highest amount of the yield stress. The strengthening mechanisms mentioned earlier can be considered as the main factors of the improvement. Regarding the amount of the yield stress in the both tensile and compressive tests, lower amount was observed in the compression test for all the samples. This asymmetry behavior in tension and compression is due to the texture of HCP crystals in the forged samples. As it was explained before, the *C*-axis of the HCP crystals is approximately parallel to the forging direction. In HCP lattice, the most common deformation twinning mode, i.e. tensile twinning $\{10\bar{1}2\}$, is activated under compressive loading perpendicular to the *C*-axis or tensile loading parallel to that [42,44]. Considering the loading direction during the compression test, the compressive loading perpendicular to the *C*-axis activates the twinning mechanism, resulting in the yield stress reduction [2,42,45].

The ductility of the composite materials is increased by more than 29% compared with that of the alloy ones. Considering the maximum strains in the tensile test, ductility is improved significantly under the compressive loading for both materials. Firstly, cracks and pores inside the materials closed during the compression test. Secondly, the

activation of twinning mechanism under the compressive loading improved the formability of the samples. However, the specimens were fractured at 45° (relative to the loading direction), indicating a brittle behavior of the materials.

### 3.5 High cycle fatigue

Figure 9 illustrates the obtained S−N fatigue curves for AZ31B and AZ31B/1.5vol.%$Al_2O_3$ composite samples with low and high amounts of applied strains.

As shown in Fig. 9(a), at a constant stress amplitude, the alloy samples from HAS zone offer the highest lifetime, while the composite samples generally exhibit a lifetime between AZ31B-LAS and AZ31B-HAZ. Moreover, by decreasing the stress amplitudes, the difference between composite specimens and alloy samples extracted from LAS zone is diminished.

Fatigue behavior of the alloys is usually related to their uniaxial tensile and compressive behaviors, although based on the previous studies such connection does not necessarily exist for metal matrix composites [11]. Similar to the tensile and compression tests, the composite samples are not sensitive to the applied strain. But unlike those tests, AZ31B samples extracted from HAS zone show a more desirable behavior in the high cycle regime. The amount of the porosity in the samples could be the most possible responsible for this behavior. According to Table 2, the porosity of the AZ31B workpiece is reduced after forging process, dramatically. So, the porosity of this sample has a more sensitivity to the applied strain in comparison with the case of the composite. These pores and cavities act as prone crack initiation points and decrease the required time for initiation of the cracks, which is considered as the most part of the fatigue life in high cycle regime. In this regime and for defect-free materials, it is expected that the fatigue crack initiation takes the most part of the fatigue life (up to 90% at low stress amplitude), in

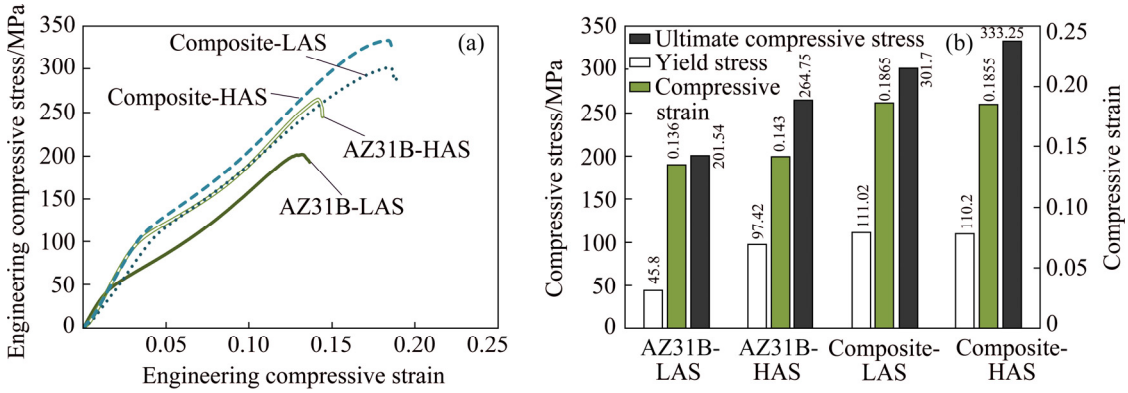


**Fig. 8** Compressive behavior of forged alloy and composite specimens: (a) Engineering compressive stress−strain curves in two different strain regions (LAS and HAS); (b) Yield stress, ultimate compressive stress and compressive strain

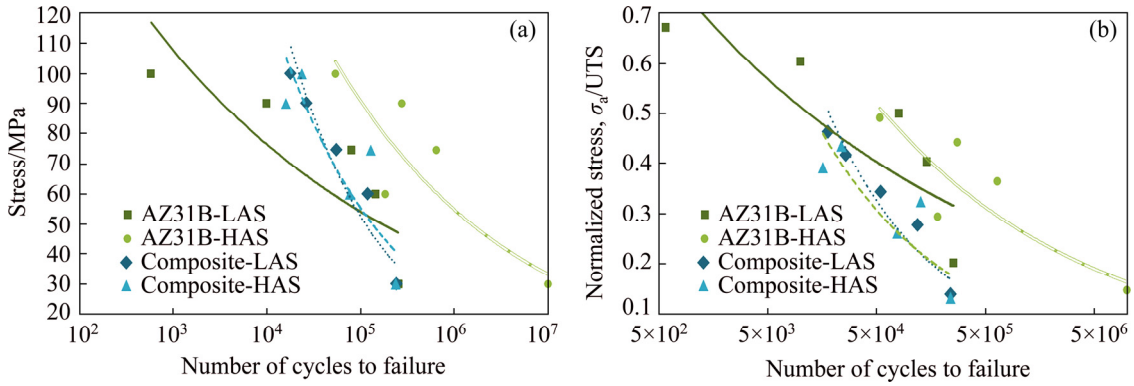


**Fig. 9** High cycle fatigue results of forged alloy and composite samples: (a) S−N curves; (b) Normalized stress amplitude vs number of cycles to failure ($\sigma_a$ is the stress amplitude)

comparison with the crack propagation step. However, the presence of different microstructural defects such as macro and micro shrinkage voids, pores of entrapped gases, micro-cracks, and particle agglomerations would reduce the duration of the crack initiation step (due to stress concentration around them) to a very short range and consequently reduce the fatigue lifetime [46]. Thus, the applied strain is not enough to enclose the existing pores and voids in the composite. However, applying more plastic strains (such as using closed-die forging process or extrusion) could improve HCF behavior of the composite [21].

Another highlight point in the tests is the scattering of the results for all the specimens. The main reason for that is the inhomogeneity of the microstructures and the amount of existing porosity. Although the as-cast microstructures are modified and refined by the open-die hot-forging process, the dynamic recrystallization occurs partially due to the relatively high strain rate and the nature of the radial forging.

Since metals with HCP crystalline structure, such as magnesium and its alloys, are unlikely to have an infinite fatigue life, their endurance limits are considered in the stress amplitudes corresponding to certain passed cycles (typically $1\times10^7$ cycle). Based on the obtained S−N curves, the AZ31B-HAZ sample lasts over $1\times10^7$ cycles at 30 MPa, which is considered as its endurance limit.

Normalized stress amplitude ($\sigma_a$/UTS) versus the number of cycles to failure curves are shown in Fig. 9(b). According to the curves, the composite samples show a demoted high cycle fatigue behavior compared with the AZ31B-LAS samples. It can be concluded that the enhancement of the UTS in the composite samples has a considerable effect on the improvement of their fatigue behavior. Furthermore, none of the samples has an endurance limit at a stress amplitude more than 20% of their UTS. Table 3 presents the parameters of Basquin's equation using the results of high cycle fatigue of the S−N curves and the least squares method.

The exponent $b$ is a very sensitive parameter with a close dependency on the material. Higher exponent absolute values or in other words steeper slopes in S−N curves exhibit less sensitivity of the fatigue life to stress amplitudes, which can be observed for the composite samples.

**Table 3** Parameters of Basquin's equation obtained from S−N curves

| Equation | Sample | $\sigma_f'$ | $b$ | $R$-squared value ($R^2$) |
|---|---|---|---|---|
| $\sigma_a=\sigma_f'N^b$ | AZ31B-HAS | 1124.9 | −0.219 | 0.80 |
| | AZ31B-LAS | 302.05 | −0.149 | 0.61 |
| | Composite-HAS | 3191 | −0.352 | 0.70 |
| | Composite-LAS | 6919.9 | −0.424 | 0.90 |

$\sigma_f'$ is the fatigue strength coefficient, $N$ is the number of cycles to failure, and $b$ is the fatigue strength exponent

### 3.6 Fractography

The fracture surfaces of the forged alloy and composite specimens after tensile test are shown in Fig. 10. According to Fig. 10, the fracture surfaces contain a combination of brittle (intergranular and transgranular) and ductile fractures. AZ31B-LAS sample shows large intergranular fracture features with river patterns, while more voids with few shallow dimples are observed in the AZ31B-HAS specimen. More intergranular failure modes in the composite samples result in smaller intergranular fracture features, indicating the presence of finer grains in the matrix. In addition, more dimples can be found in the fracture surfaces of the composite material, showing more ductile behavior in comparison with the AZ31B samples.

Figure 11 shows different defects on fracture surfaces of the forged specimens under tensile loading. The presence of the micro-cracks shows a local brittle behavior which can be intensified by existence of precipitates. In addition, there are different voids created during casting process in all the samples. Another defect which can be observed in the composite samples is nanoparticle agglomerations. Although bulk forming process decreases the agglomerations inside the matrix, open-die forging is not able to diminish all of them. These defects would decrease the formability of the forged composite samples. It should be noted that applying more plastic strain could decrease the mentioned defects more significantly.

Figure 12 illustrates the macroscopic views of the fatigue fracture surfaces of the forged alloy and composite at a stress amplitude of 100 MPa, showing crack propagation regions (CPR) and sudden fracture (SF). In all the samples, there are three different regions including crack initiation, crack propagation, and sudden fracture regions. The

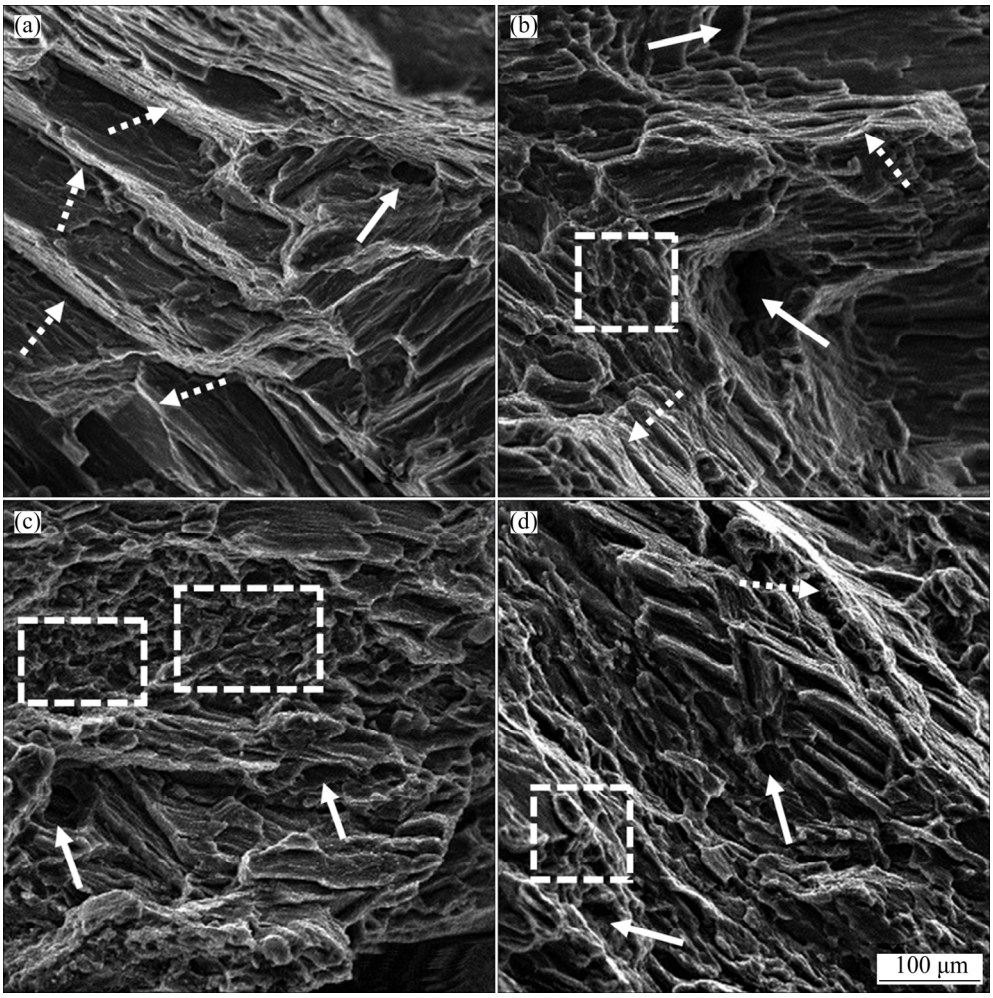


**Fig. 10** Fracture surfaces of forged samples under tensile loading: (a) Local brittle failure mechanism in AZ31B-LAS with large cleavage steps, microscopic voids (arrows), and river pattern (dotted arrows); (b) Ductile−brittle fracture features with combination of cleavage steps, river pattern (dotted arrows) and microscopic voids (arrows) with areas of dimples (dashed-line rectangle) in AZ31B-HAS; (c) Voids (arrows) and local ductile feature of multi-sized dimples (dashed-line rectangles) in composite-LAS; (d) River pattern (dotted-line arrow), microscopic voids (arrow), and shallow dimples (dashed-line rectangle) in composite-HAS

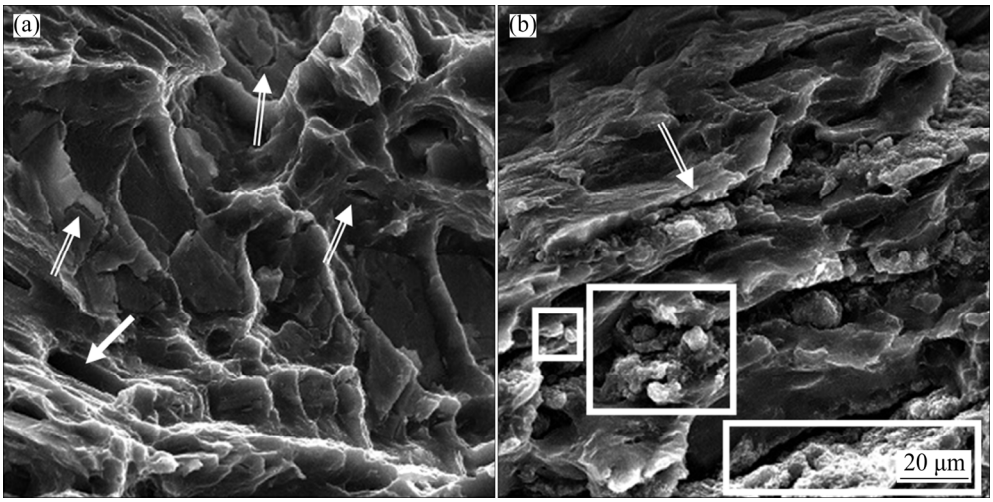


**Fig. 11** Different defects on fracture surfaces of forged samples under tensile loading: (a) Microscopic voids (arrow) and micro-cracks (double-line arrows); (b) Micro-cracks (double-line arrow) and brittle lamellar fracture structures around nanoparticle agglomerations and secondary phases (white rectangles)

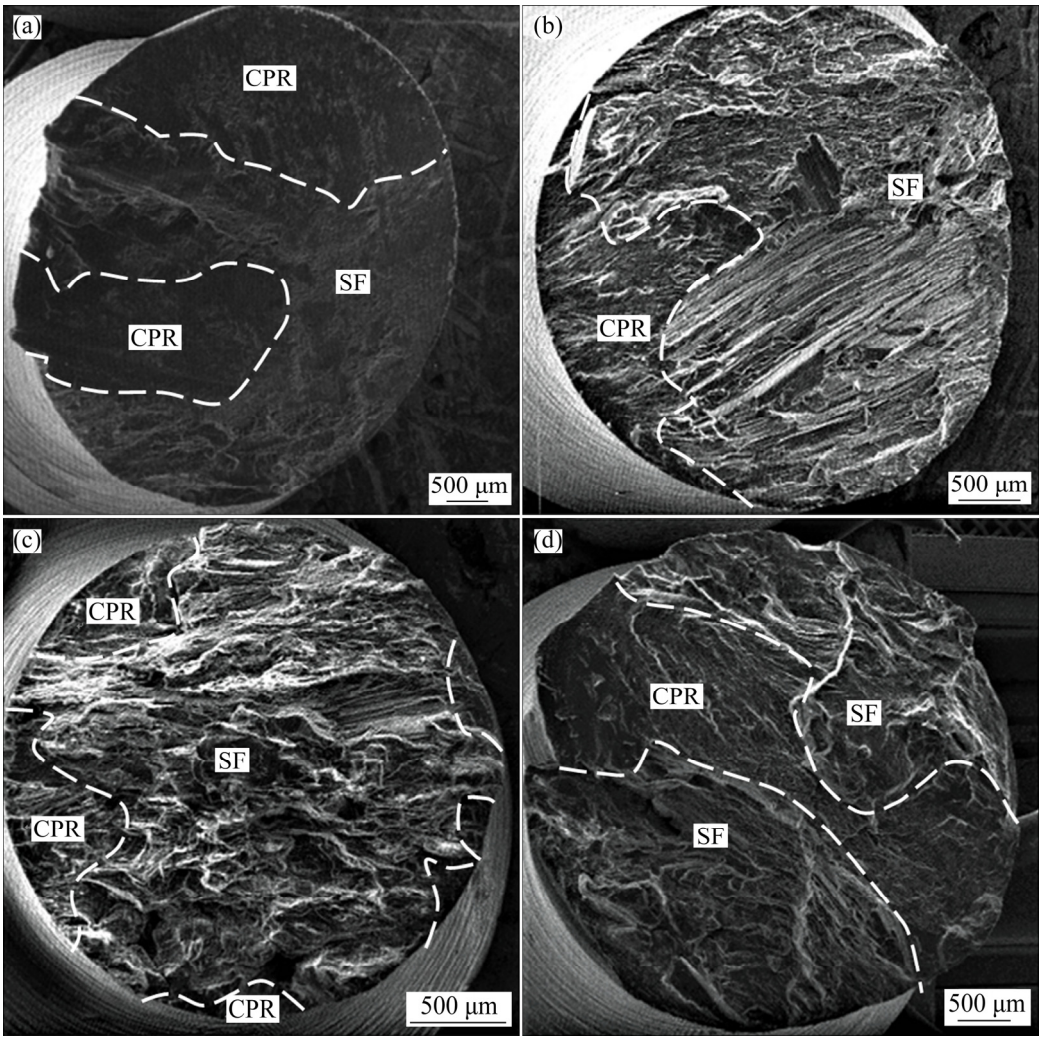


**Fig. 12** Macroscopic views of fatigue fracture surfaces of forged samples at stress amplitude of 100 MPa: (a) AZ31B-LAS; (b) AZ31B-HAS; (c) Composite-LAS; (d) Composite-HAS

dark and smooth areas relate to the crack initiation regions, which are usually located near the edges of the fatigue sample due to stress distribution during the rotating-bending fatigue tests. These regions are followed by brighter crack propagation regions including river patterns or striations. Finally, the sudden fracture regions are surrounded by tear ridges and have rough surfaces. The ratio of the sudden fracture area to the total area can represent the ratio of the applied stress amplitude to the UTS. In fact, since composite-HAS sample has a higher UTS than composite-LAS one, it is expected that a smaller sudden fracture region can be observed in this sample. Figures 13 shows the microscopic views of the fatigue fracture surfaces of forged samples under stress amplitude of 100 MPa at higher magnifications.

The Existence of porosities and voids, river patterns, micro-cracks, tear ridges, striations, and striation pockets indicates a mixture of brittle and ductile behaviors. Furthermore, different matrix delaminations are remarkable in both AZ31B-LAS and composite-LAS, while they can rarely be observed in the samples extracted from HAS zones. In the composite-LAS, the fatigue striation is followed by delamination of the matrix [7]. On the other hand, striation pockets are visible in the composite-HAS sample, showing local ductility in the matrix [41]. Although adding nano-sized particles improved UTS of the matrix and could change the crack path (resulting in a longer fatigue life) [6], the porosities and particle agglomerations acted as crack initiation and stress concentration points and degraded the fatigue behavior of the composites.

Macroscopic views of the fatigue fracture surfaces of the forged samples at a stress amplitude of 30 MPa are shown in Fig. 14. Considering the

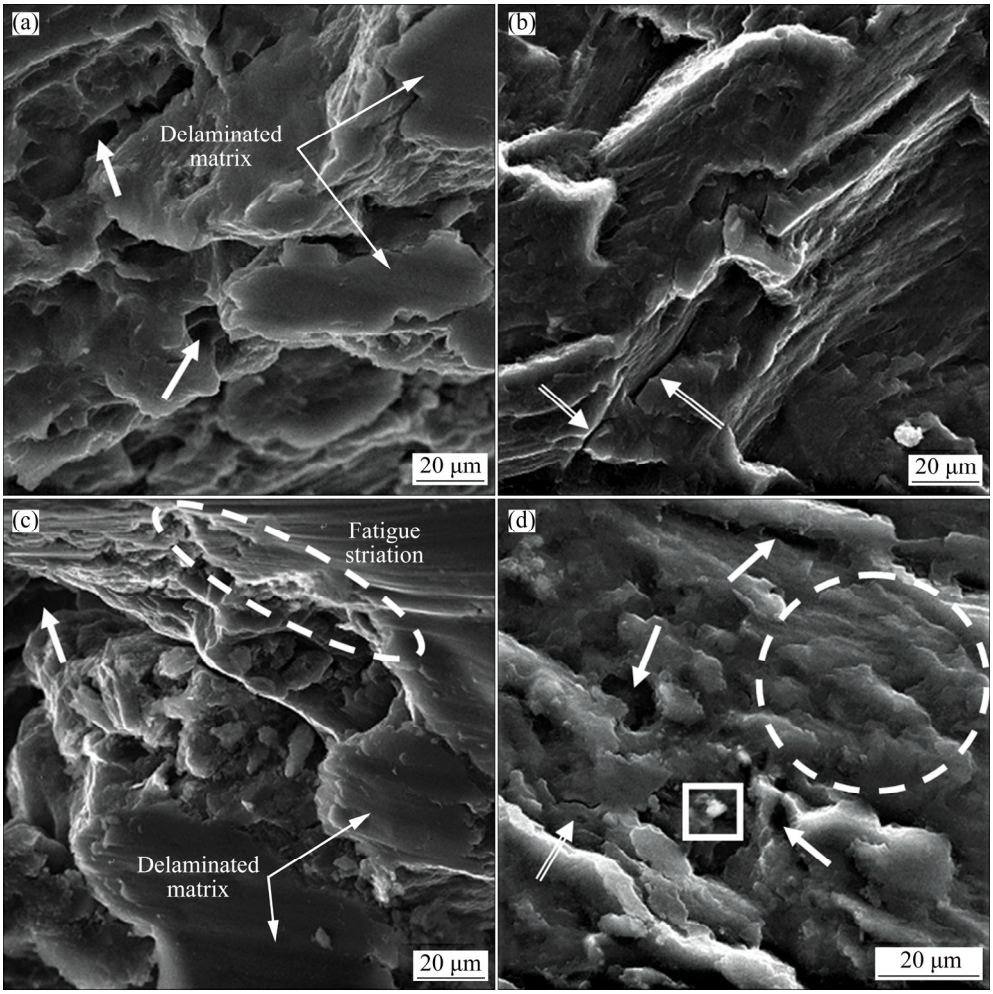


**Fig. 13** Microscopic views of fatigue fracture surfaces of forged samples at stress amplitude of 100 MPa: (a) Voids (arrows) and delaminated matrix at CPR in AZ31B-LAS; (b) Micro-cracks (double-line arrows) in AZ31B-HAS; (c) Voids (arrow), fatigue striation restricted by tear ridges (dashed-line oval), and large delaminated matrix in CPR of composite-LAS; (d) Micro-cracks (double-line arrow), voids (arrows), reinforcing particles agglomeration (box), and striation pockets (dashed-line circle) in composite-HAS

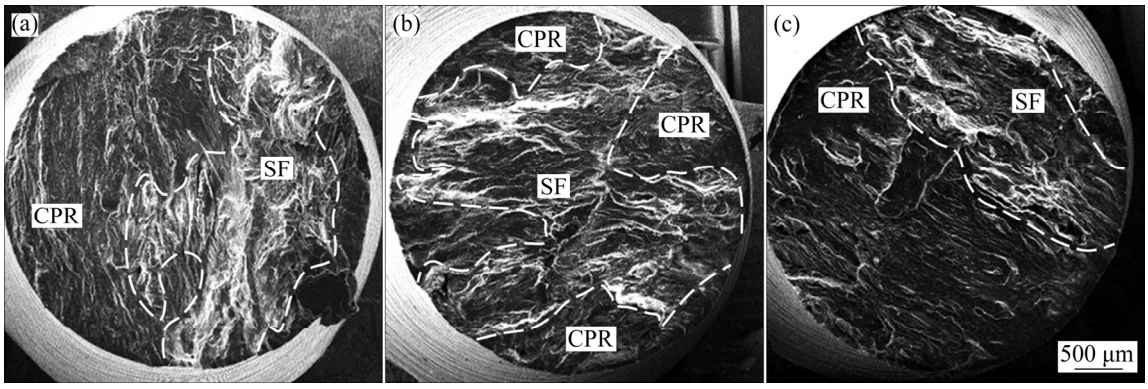


**Fig. 14** Macroscopic views of fatigue fracture surfaces of forged samples at stress amplitude of 30 MPa: (a) AZ31B-LAS; (b) Composite-LAS; (c) Composite-HAS

fracture surfaces at the stress amplitude of 100 MPa, larger crack propagation regions can be observed in the samples subjected to the stress amplitude of 30 MPa. In fact, the ratio of the sudden fracture area to the total area is decreased by reduction of the applied stress amplitude. Figure 15 shows the

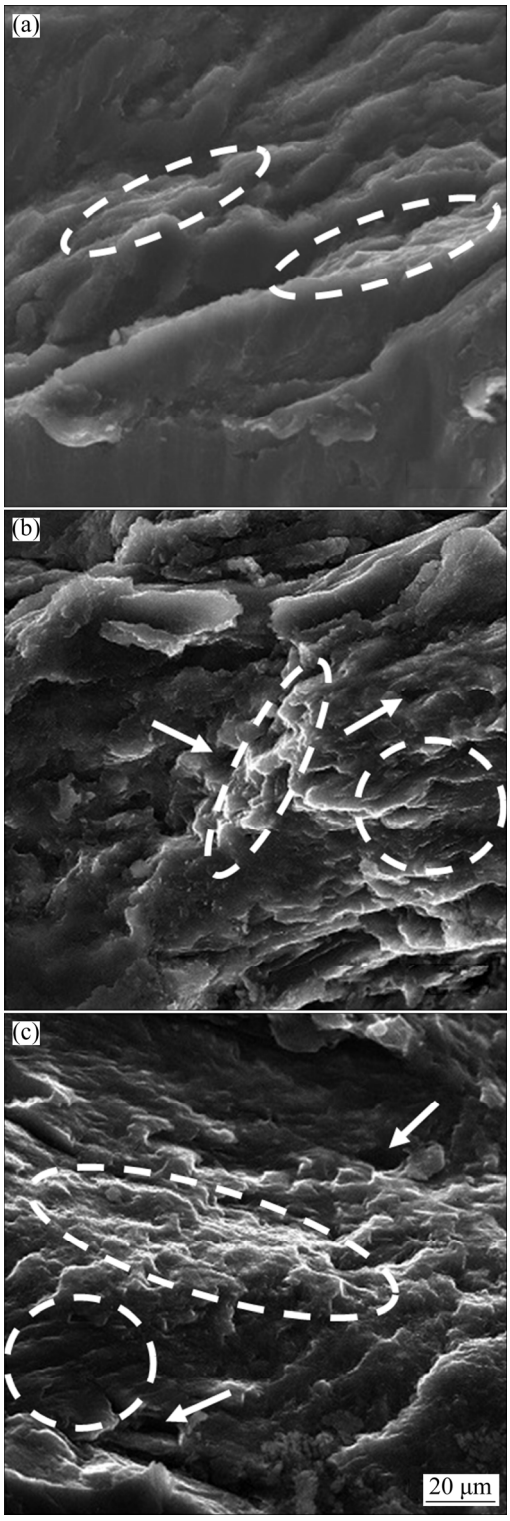


**Fig. 15** Microscopic views of fatigue fracture surfaces of forged samples at stress amplitude of 30 MPa: (a) Fracture through multi-sized DRXed grains and tear ridges (dashed-line ovals) in AZ31B-LAS; (b) Voids (arrows), striation pockets (dashed-line circle), and tear ridges (dashed-line oval) in composite-LAS; (c) Voids (arrows), striation pockets (dashed-line circle), and tear ridges (dashed-line oval) in composite-HAS

microscopic views of the fatigue fracture surfaces of the forged samples at a stress amplitude of 30 MPa. It should be noted that since the AZ31B-HAS sample has an infinite life under the stress amplitude of 30 MPa, no fracture surface is shown for this sample in Figs. 14 and 15.

According to Fig. 15(a), cleavage fracture surfaces can be observed in the AZ31B-LAS sample. From the microscopic aspect, the presence of the large laminated surfaces along with smaller brittle fracture surfaces is due to the non-uniformity of the grains, resulted from the partially DRXed microstructure. Although the tear ridges are a sign of brittle fracture in all the samples, the existence of striation pockets shows a local ductile behavior in the composite specimens. Thus, the fracture surfaces of the composites demonstrate a mixture of brittle and local ductile behaviors under cyclic loading, which is due to the presence of nano-sized $Al_2O_3$ particles.

## 4 Conclusions

(1) The open-die hot-forging process decreased the porosity by 71% and 19% for both ZA31B alloy and ZA31B/1.5vol.%$Al_2O_3$ composite workpieces, respectively, although the reduction was very more considerable in the alloy one.

(2) The as-cast composite samples possessed finer and more uniform grains due to the presence of the ceramic particles as grains nucleation sites and the pinning effect. During the hot-forging process, dynamic recrystallization (DRX) generated finer grains in both materials. However, the DRX happened partially, especially in the alloy samples.

(3) Adding the nano-sized ceramic particles to the magnesium alloy and applying more strain during forging process led to the enhancement of the microhardness of the samples.

(4) In similar regions, the ultimate tensile strength and the maximum tensile strain of the composite were enhanced by 45% and 23%, respectively, in comparison with the forged alloy sample. In the case of the compression test, these amounts were 50% and 37%, respectively. Against the alloy samples, increasing the applied strain did not have a considerable effect on the tensile and compressive behaviors of the composites.

(5) The results of the high cycle fatigue tests indicated that the composite fatigue life was not

very sensitive to the applied strain. Both composite samples showed a fatigue behavior between AZ31B-LAS (low applied strain) and AZ31B-HAS (high applied strain) samples. Only AZ31B-HAS sample showed an endurance limit (in $1\times10^7$ cycle) at a stress amplitude of 30 MPa.

(6) High amount of porosity in the composite (as potential crack initiation points) can be considered as the most possible reason for the fatigue life reduction in HAS regions.

(7) Investigation of the tensile fracture surfaces showed a combination of brittle and ductile fractures in both alloy and composite samples, although the brittle mechanism was more dominated. In comparison with the AZ31B samples, the composite fracture surfaces indicated smaller intergranular fracture features with more voids and few shallow dimples.

(8) A mixture of brittle and ductile behaviors was observed in the fracture surfaces of the fatigue samples. Micro-voids and striation pockets were more obvious in the composite samples, showing a local ductile behavior in the matrix.

## References


[1] YOU S H, HUANG Y D, KAINER K U, HORT N. Recent research and developments on wrought magnesium alloys [J]. Journal of Magnesium and Alloys, 2017, 5(3): 239−253.

[2] TOSCANO D, SHAHA S K, BEHRAVESH B, JAHED H, WILLIAMS B. Effect of forging on microstructure, texture, and uniaxial properties of cast AZ31B alloy [J]. Journal of Materials Engineering and Performance, 2017, 26(7): 3090−3103.

[3] SABET A S, JABBARI A H, SEDIGHI M. Microstructural properties and mechanical behavior of magnesium/ hydroxyapatite biocomposite under static and high cycle fatigue loading [J]. Journal of Composite Materials, 2018, 52(13): 1711−1722.

[4] TOSCANO D, SHAHA S K, BEHRAVESH B, JAHED H, WILLIAMS B. Effect of forging on the low cycle fatigue behavior of cast AZ31B alloy [J]. Materials Science and Engineering A, 2017, 706: 342−356.

[5] GUO Wei, WANG Qu-dong, YE Bing, ZHOU Hao. Microstructure and mechanical properties of AZ31 magnesium alloy processed by cyclic closed-die forging [J]. Journal of Alloys and Compounds, 2013, 558: 164−171.

[6] TOSCANO D, SHAHA S K, BEHRAVESH B, JAHED H, WILLIAMS B, SU X. Influence of low temperature forging on microstructure and low cycle fatigue behavior of cast AZ31B Mg alloy [C]//Cham: TMS Annual Meeting & Exhibition, 2018: 267−273.

[7] MOHAMMADI S, JABBARI A H, SEDIGHI M. Mechanical properties and microstructure of Mg−$SiC_p$ composite sheets fabricated by sintering and warm rolling [J]. Journal of Materials Engineering and Performance, 2017, 26(7): 3410−3419.

[8] YUAN Qiu-hong, FU Dong-ming, ZENG Xiao-shu, YONG LIU. Fabrication of carbon nanotube reinforced AZ91D composite with superior mechanical properties [J]. Transactions of Nonferrous Metals Society of China, 2017, 27(8): 1716−1724.

[9] NARAYANASAMY P, SELVAKUMAR N. Tensile, compressive and wear behaviour of self-lubricating sintered magnesium based composites [J]. Transactions of Nonferrous Metals Society of China, 2017, 27(2): 312−323.

[10] HASHIM J, LOONEY L, HASHMI M S J. Metal matrix composites: Production by the stir casting method [J]. Journal of Materials processing technology, 1999, 92: 1−7.

[11] CHAWLA N, CHAWLA K K. Metal matrix composites [M]. 2nd ed. New York: Springer, 2013.

[12] CLYNE T, WITHERS P. An introduction to metal matrix composites [M]. Cambridge: Cambridge University Press, 1993.

[13] KOIKE J, KOBAYASHI T, MUKAI T, WATANABE H, SUZUKI M, MARUYAMA K, HIGASHI K. The activity of non-basal slip systems and dynamic recovery at room temperature in fine-grained AZ31B magnesium alloys [J]. Acta Materialia, 2003, 51(7): 2055−2065.

[14] WANG Xiao-jun, LIU Wei-qing, HU Xiao-shi, WU Kun. Microstructural modification and strength enhancement by SiC nanoparticles in AZ31 magnesium alloy during hot rolling [J]. Materials Science and Engineering A, 2018, 715: 49−61.

[15] DENG K K, WANG X J, GAN W M, WU Y W, NIE K B, WU K, ZHENG M Y, BROKMEIER H G. Isothermal forging of AZ91 reinforced with 10 vol.% silicon carbon particles [J]. Materials Science and Engineering A, 2011, 528: 1707−1712.

[16] GOH C S, WEI J, LEE L C, GUPTA M. Ductility improvement and fatigue studies in Mg−CNT nanocomposites [J]. Composites Science and Technology, 2008, 68(6): 1432−1439.

[17] LIANG Jun-hao, LI He-jun, QI Le-hua, TIAN Wen-long, LI Xue-feng, CHAO Xu-jiang, WEI Jian-feng. Fabrication and mechanical properties of CNTs/Mg composites prepared by combining friction stir processing and ultrasonic assisted extrusion [J]. Journal of Alloys and Compounds, 2017, 728: 282−288.

[18] HASSAN H A, LEWANDOWSKI J J. Effects of particulate volume fraction on cyclic stress response and fatigue life of AZ91D magnesium alloy metal matrix composites [J]. Materials Science and Engineering A, 2014, 600: 188−194.

[19] SRIVATSAN T S, GODBOLE C, QUICK T, PARAMSOTHY M, GUPTA M. Mechanical behavior of a magnesium alloy nanocomposite under conditions of static tension and dynamic fatigue [J]. Journal of Materials Engineering and Performance, 2013, 22(2): 439−453.

[20] JABBARI A H, SEDIGHI M, SABET A S. Combination of mechanical and electromagnetic stirring to distribute nano-sized $Al_2O_3$ particles in magnesium matrix composite [J]. Powder Metallurgy and Metal Ceramics, 2019, 58(5−6): 361−371.

[21] JABBARI A. H, SEDIGHI M. Investigation of electromagnetic and mechanical stirring sequence effects on production of magnesium matrix nanocomposite [J]. International Journal of Metalcasting, 2019, 14(2): 489−504.

[22] MAZAHERY A, SHABANI M. Mechanical properties of A356 matrix composites reinforced with nano-SiC particles [J]. Strength of Materials, 2012, 44(6): 686−692.

[23] KHANDELWAL A, MANI K, SRIVASTAVA N, GUPTA R, CHAUDHARI G P. Mechanical behavior of AZ31/$Al_2O_3$ magnesium alloy nanocomposites prepared using ultrasound assisted stir casting [J]. Composites (Part B): Engineering, 2017, 123: 64−73.

[24] HABIBNEJAD-KORAYEM M, MAHMUDI R, POOLE W J. Enhanced properties of Mg-based nano-composites reinforced with $Al_2O_3$ nano-particles [J]. Materials Science and Engineering A, 2009, 519(1−2): 198−203.

[25] WANG Zhao-hui, WANG Xu-dong, ZHAO Yu-xin, DU Wen-bo. SiC nanoparticles reinforced magnesium matrix composites fabricated by ultrasonic method [J]. Transactions of Nonferrous Metals Society of China, 2010, 20: 1029−1032.

[26] MIRZA F, CHEN D. A unified model for the prediction of yield strength in particulate-reinforced metal matrix nanocomposites [J]. Materials, 2015, 8(8): 5138−5153.

[27] SANATY-ZADEH A. Comparison between current models for the strength of particulate-reinforced metal matrix nanocomposites with emphasis on consideration of Hall−Petch effect [J]. Materials Science and Engineering A, 2012, 531: 112−118.

[28] PRABU S B, KARUNAMOORTHY L, KATHIRESAN S, MOHAN B. Influence of stirring speed and stirring time on distribution of particles in cast metal matrix composite [J]. Journal of Materials Processing Technology, 2006, 171(2): 268−273.

[29] AHMAD S N, HASHIM J, GHAZALI M I. The effects of porosity on mechanical properties of cast discontinuous reinforced metal–matrix composite [J]. Journal of Composite Materials, 2005, 39(5): 451−466.

[30] NIE K B, WU K, WANG X J, DENG K K, WU Y W, ZHENG M Y. Multidirectional forging of magnesium matrix composites: Effect on microstructures and tensile properties [J]. Materials Science and Engineering A, 2010, 527: 7364−7368.

[31] AL-SAMMAN T, GOTTSTEIN G. Dynamic recrystallization during high temperature deformation of magnesium [J]. Materials Science and Engineering A, 2008, 490: 411−420.

[32] KAYA A A, DUYGULU O, YUCEL O, ELIEZER D. Effect of grain size on necklace formation of magnesium alloys [J]. Materials Science Forum, 2007, 546: 233−236.

[33] LASER T, NÜRNBERG M R, JANZ A, HARTIG C, LETZIG D, SCHMID-FETZER R, BORMANN R. The influence of manganese on the microstructure and mechanical properties of AZ31 gravity die cast alloys [J]. Acta Materialia, 2006, 54(11): 3033−3041.

[34] STANFORD N, ATWELL D. The effect of Mn-rich precipitates on the strength of AZ31 extrudates [J]. Metallurgical and Materials Transactions A, 2013, 44(10): 4830−4843.

[35] NIA A A, NOURBAKHSH S H. Microstructure and mechanical properties of AZ31/SiC and AZ31/CNT composites produced by friction stir processing [J]. Transactions of the Indian Institute of Metals, 2016, 69(7): 1435−1442.

[36] OMIDI N, JABBARI A H, SEDIGHI M. Mechanical and microstructural properties of titanium/hydroxyapatite functionally graded material fabricated by spark plasma sintering [J]. Powder Metallurgy, 2018, 61(5): 417−427.

[37] CASATI R, VEDANI M. Metal matrix composites reinforced by nano-particles—A review [J]. Metals, 2014, 4(1): 65−83.

[38] NGUYEN Q B, GUPTA M. Enhancing compressive response of AZ31B magnesium alloy using alumina nanoparticulates [J]. Composites Science and Technology, 2008, 68(10−11): 2185−2192.

[39] DENG Kun-kun, SHI Ju-yan, WANG Cui-ju, WANG Xiao-jun, WU Ye-wei, NIE Kai-bo, WU Kun. Microstructure and strengthening mechanism of bimodal size particle reinforced magnesium matrix composite [J]. Composites (Part A): Applied Science and Manufacturing, 2012, 43(8): 1280−1284.

[40] CHEN Gang, WAN Jia, HE Ning, ZHANG Hong-ming, HAN Fei, ZHANG Yu-min. Strengthening mechanisms based on reinforcement distribution uniformity for particle reinforced aluminum matrix composites [J]. Transactions of Nonferrous Metals Society of China, 2018, 28(12): 2395−2400.

[41] SRIVATSAN T S, GODBOLE C, PARAMSOTHY M, GUPTA M. The role of aluminum oxide particulate reinforcements on cyclic fatigue and final fracture behavior of a novel magnesium alloy [J]. Materials Science and Engineering A, 2012, 532: 196−211.

[42] PARK S H, LEE J H, MOON B G, YOU B S. Tension–compression yield asymmetry in as-cast magnesium alloy [J]. Journal of Alloys and Compounds, 2014, 617: 277−280.

[43] LUKÁČ P, TROJANOVÁ Z. Influence of grain size on ductility of magnesium alloys [J]. Materials Engineering, 2011, 18(3): 110−114.

[44] HONG S G, PARK S H, LEE C S. Role of $\{10\bar{1}2\}$ twinning characteristics in the deformation behavior of a polycrystalline magnesium alloy [J]. Acta Materialia, 2010, 58(18): 5873−5885.

[45] YANG Shu, ZHANG Xi-yan, YU Jiang-ping, LI Tan, YIN Rui-sen, QING Liu. Tensile behaviors of fatigued AZ31 magnesium alloy [J]. Transactions of Nonferrous Metals Society of China, 2018, 28(5): 896−901.

[46] POTZIES C, KAINER K U. Fatigue of magnesium alloys [J]. Advanced Engineering Materials, 2004, 6(5): 281−289.

# 纳米 $Al_2O_3$ 增强颗粒对热锻 AZ31B 镁合金单轴及高周疲劳性能的影响

M. DAREINI, A. H. JABBARI, M. SEDIGHI

School of Mechanical Engineering, Iran University of Science and Technology, Narmak, Tehran 1684613114, Iran

**摘　要：**研究热锻工艺对 AZ31B 合金和 AZ31B/1.5vol.%$Al_2O_3$ 纳米复合材料在静态和循环加载下的显微组织和力学性能的影响。首先将铸态合金和复合材料在 450 °C 下进行均匀化热处理，然后在 450 °C 下进行开式模锻。结果表明，增强颗粒的存在有利于晶粒细化和改善动态再结晶。锻造工艺能更有效地消除铸态合金工件中的孔隙。与铸态和锻态合金试样相比，锻态复合材料的显微硬度分别提高 80%和 16%。与锻态合金的相似区域相比，锻态复合材料的极限抗拉强度和最大拉伸应变分别提高 45%和 23%，极限压缩强度和最大压缩强度分别提高 50%和 37%。复合材料在低应变区的疲劳寿命提高，而在高应变区的疲劳寿命降低。与 AZ31B 试样不同，复合材料的拉伸、压缩和高周疲劳行为对施加应变的敏感性较低，这与试样在热锻前后的孔隙率有关。

**关键词：**镁基纳米复合材料；AZ31B 合金；纳米氧化铝；开式热锻；高周疲劳；力学性能；显微组织演变

**(Edited by Wei-ping CHEN)**